

Final Draft
of the original manuscript:

aus der Beek, T.; Menzel, L.; Rietbroek, R.; Fenoglio-Marc, L.; Grayek, S.;
Becker, M.; Kusche, J.; Stanev, E.V.:

**Modeling the water resources of the Black and Mediterranean Sea
river basins and their impact on regional mass changes**

In: Journal of Geodynamics (2011) Elsevier

DOI: 10.1016/j.jog.2011.11.011

1 **Modeling the water resources of the Black and** 2 **Mediterranean Sea river basins and their impact on** 3 **regional mass changes**

4 **T. aus der Beek^{1,2}, L. Menzel¹, R. Rietbroek³, L. Fenoglio-Marc⁴, S. Grayek^{5,6}, M.**
5 **Becker⁴, J. Kusche³, E. Stanev^{5,6}**

6
7 ¹Department of Geography, Heidelberg University, Germany

8 ²Center for Environmental Systems Research, University of Kassel, Germany

9 ³Institute of Geodesy and Geoinformation, University of Bonn, Germany

10 ⁴Institute of Physical Geodesy, University of Darmstadt, Germany

11 ⁵Institute for Chemistry and Biology of the Sea, University of Oldenburg, Germany

12 ⁶Institute for Coastal Research, GKSS Research Center, Germany

13 Correspondence to: T. aus der Beek (Wilhelmshöher Allee 47, 34109 Kassel, Germany;

14 Email: ausderbeek@usf.uni-kassel.de; Telephone: 0049-5618046121; Fax: 0049-5618046116)

15 **Abstract**

16 For the first time, a dedicated release of the hydrology and water use model WaterGAP3, has been developed to
17 spatially explicit calculate hydrological fluxes within river basins draining into the Mediterranean and Black Sea.
18 The main differences between the new regional version of the global WaterGAP3 model and the previously
19 applied global version WaterGAP2 can be found in the spatial resolution, snow modeling, and water use
20 modeling. Comparison with observations shows that WaterGAP3 features a more realistic representation of
21 modeled river runoff and inflow into both seas. WaterGAP3 generates more inflow to both seas than
22 WaterGAP2. In the WaterGAP3 simulation, contributions to the total runoff into the Black Sea from individual
23 discharge regions show in general a good agreement to climatology derived runoff, but lesser importance of
24 Georgian rivers for the basin's water. After the successful model validation WaterGAP3 has been applied to
25 correct estimates of seawater mass derived from the GRACE gravity mission and to account for freshwater
26 inflow into both basins. The performance of the WaterGAP3 regional solution has been evaluated by comparing
27 the seawater mass derived from GRACE corrected for the leakage of continental hydrology, to an independent
28 estimate derived from steric-corrected satellite altimetry with steric correction from regional oceanographic
29 models. The agreement is higher in the Mediterranean Sea than in the Black Sea. Results using WaterGAP3 and
30 WaterGAP2 are not significantly different. However the agreement with the altimetry-derived results is higher
31 using WaterGAP2, due to the smaller annual amplitude of the continental hydrology leakage from WaterGAP3.
32 We conclude that the regional model WaterGAP3 is capable of realistically quantifying water mass variation in
33 the region, further developments have been identified.

34
35 **Keywords:** GRACE, mass transport, oceanography, altimetry, WaterGAP

36 **1 Introduction**

37 In terrestrial hydrology, the separation of water in the numerous storage compartments is a
38 highly complex problem. The heterogeneous nature of soil and topography results in water
39 storage variations which can vary strongly in the spatial domain. At the same time,
40 precipitation, evapotranspiration, water routing and anthropogenic water use all play a strong
41 role in the (re-)distribution of water. Often depending on integrative measurements, such as
42 observed river runoff, the use of models in hydrology is indispensable in understanding the
43 (re-)distribution of water. Their utilization is twofold; on the one hand, they provide estimates
44 of water storage where observations alone do not suffice, while on the other hand they
45 provide an opportunity to study the physics of the system by means of simulations. The
46 validation/calibration of the hydrological models depends on independent observations. River
47 gauges are traditionally used to calibrate the models, but the data is sparse or unavailable.
48 Since the launch of the Gravity Recovery and Climate Experiment (GRACE), large scale
49 measurements of total water storage have been available (Schmidt et al. 2006). When used in
50 conjunction with in situ observations, GRACE data have the potential to significantly
51 improve our understanding of hydrological processes and the global water cycle and provide
52 opportunities for model calibration (Werth 2010). A comprehensive overview of hydrological
53 and land surface models dealing with GRACE derived mass variations is given by Güntner
54 (2008).

55 In this study, a regional version of the global hydrology and water use model WaterGAP3
56 (Aus der Beek et al. 2011) has been developed, which includes all river basins draining into
57 the Mediterranean and Black Sea. In addition to the increased spatial resolution (5 arc
58 minutes), special attention was given to improved process algorithms (e.g. snow hydrology
59 and flow velocity) and more detailed anthropogenic water use modules, which is a significant
60 factor in the heavily populated drainage basins (Aus der Beek et al. 2010). In order to evaluate
61 the performance of WaterGAP3 and the goodness of its results, modeled river runoff has been
62 compared to observed river runoff from gauging stations available in the study region.
63 Furthermore, to grade the new regional WaterGAP3 model version, its results have also been
64 compared to those from WaterGAP2 and a land surface model. After the successful
65 verification of the WaterGAP3 model results, monthly maps of total water storage (TWS)
66 have been produced. We then use this TWS data to correct the water mass variation estimated
67 by GRACE (Chambers 2006, Fenoglio-Marc et al., 2006, 2007). On the other hand, also

68 steric-corrected altimetry gives an estimation of seawater mass. The consistency between the
69 two estimates is affected by the continental hydrological leakage and steric corrections
70 (Fenoglio-Marc et al. this issue), therefore the modeled TWS can be evaluated through the
71 comparison. Here, we compare steric-corrected altimetry with GRACE corrected by using the
72 regional WaterGAP3 and the global WaterGAP2 models.

73 **2 Material and Methods**

74 **2.1 Regional modeling of hydrology using WaterGAP3**

75 The hydrology and water use model applied in this study is WaterGAP3 (Water – Global
76 Assessment and Prognosis). It is a further developed version of the well known global
77 hydrology and water use model WaterGAP2 (Alcamo et al. 2003, Döll et al. 2003).
78 WaterGAP3 operates on the global scale but for each continent separately, whereas a special
79 landmask has been developed for this study, as the study region includes parts of three
80 continents (Europe, Africa, and Asia). Thus, the landmask includes all river basins draining
81 into the Black and Mediterranean Sea. In addition to the increase in spatial resolution from
82 0.5° (~50 km x 50 km) to 5' (~7 km x 7 km) (Verzano 2009) also some hydrological process
83 descriptions have been improved in WaterGAP3, such as snow (Verzano & Menzel 2009) and
84 permafrost modeling (Aus der Beek & Teichert 2008), flow velocity (Verzano et al. 2005),
85 and the water use modules (Aus der Beek et al. 2010; Flörke et al. 2011).

86 WaterGAP3 calculates daily water fluxes and anthropogenic water abstractions for all river
87 basins draining into the Mediterranean and Black Sea (see Figure 1) on a 5 by 5 arc minutes
88 grid (longitude and latitude). For each grid cell it takes into account spatially distributed
89 physiographic information about elevation, slope, hydrogeology, land cover and soil
90 properties, as well as location and extent of lakes, wetlands, and reservoirs. The
91 upstream/downstream relationship among the grid cells is defined by a global drainage
92 direction map (DDM) which indicates the drainage direction of surface water (Lehner et al.
93 2008). Five water use models within the WaterGAP framework (Flörke and Alcamo 2005,
94 Alcamo et al. 2003, Döll and Siebert 2002) take into account water consumption by
95 households, manufactures, energy production industries, livestock, and irrigation, as the
96 consideration of water uses is crucial for a realistic representation of the water balance of
97 most river basins. The aim of WaterGAP3 is to simulate the characteristic behaviour of the
98 terrestrial water cycle in order to estimate total water storage (TWS) for each grid cell and

99 river basin. Herein, TWS is defined as the sum of all potential water storages: rivers,
100 groundwater, soil water, canopy water, snow, lakes, and wetlands. River runoff is calibrated
101 and validated with a single tuning parameter (Döll et al. 2003) against 63 stations of observed
102 river flow (GRDC 2004). Climate forcing data used in this study have been compiled from
103 station data and regionalized by the Climate Research Unit (CRU) of the University of East
104 Anglia, Norwich, U.K. (versions TS 1.2 and TS 2.1, Mitchell and Jones, 2005). CRU data
105 covers the time period from 1901 to 2002 in 10' and 0.5° resolution and monthly time steps,
106 providing nine climatic parameters, e.g. precipitation, air temperature, cloud cover, etc.. For
107 the time period 2003 to 2009 climate forcing data has been provided by the ECMWF
108 (European Centre for Medium Weather Forecast) in 0.35° (until January 2006) and 0.22°
109 resolution. Precipitation data for this time period originates from the GPCC (Global
110 Precipitation and Climate Center) and features a spatial resolution of 0.5° (until December
111 2007) and 1° (Rudolf & Schneider 2005). All climate input data has been converted to the 5'
112 WaterGAP3 grid. Each 5' cell is linked to a, e.g., 0.5 cell based on geographical location of
113 the center of the 5' cell. Thus, the climate data has only been remapped to the 5' grid, and not
114 re-interpolated.

115 Hydrological modeling has been conducted for the time period 1901 to 2009. This ensures an
116 optimal utilization of station data for the calibration of WaterGAP3, as observed runoff data
117 generally is scarce after 2002. Only river basins draining into the Mediterranean and Black
118 Sea have been selected for this regional version of WaterGAP3 (see Figure 1). River basins,
119 which do not drain into the Black or Mediterranean Sea, but which are located within other
120 river basins that actually do drain into the Black or Mediterranean Sea, such as in Turkey, the
121 Balkans, or in the Nile basin, are considered as inland sinks. Thus, they are excluded from the
122 model set-up.

123

124 To test the performance of the regional WaterGAP3 model, its results are being compared to
125 the results from the models WaterGAP2 and GLDAS (Global Land Data Assimilation
126 System) (Rodell et al. 2004). GLDAS drives four different land surface models (LSMs):
127 CLM, MOSAIC, NOAH, VIC which simulate the transfer of mass, energy, and momentum
128 between the soil and vegetation surfaces and the atmosphere. In this study, routed river runoff
129 data from all four LSMs has been provided for the Danube and Dnieper rivers (Zaitchik
130 2010). To simplify the comparison an unweighted mean of all four GLDAS LSMs has been
131 applied. Furthermore, the WaterGAP3 results are also being compared to values from

132 literature (Ludwig et al. 2009; Jaoshvili 2002) and climatological estimates (Grayek et al
133 2010).

134

135 To test the performance of the regional WaterGAP3 model in computing the continental
136 hydrology leakage on GRACE, the global models WaterGAP2, Land Dynamics (LaD) Fraser
137 (Mill and Shmakin, 2002) and Community Land Model of the Global Data Assimilation
138 System (GLDAS-CLM) (Rodell et al., 2004) have been used.

139 **2.2 GRACE gravimetry and Jason-1 multi-satellite altimetry**

140 In order to assess the influence of the hydrological models as corrections to the basin
141 averaged ocean mass estimated from GRACE, we have constructed time series from GRACE
142 gravimetry on the Mediterranean and on the Black Sea basins. The hydrological leakage has
143 been estimated by converting the total water storage from the hydrological models to the
144 spectral domain and computing monthly filtered basin averages in the same way as for
145 GRACE. The general procedure is outlined below, more details on the processing can be
146 found in Fenoglio-Marc et al. (this issue).

147

148 We have used the GRACE data (GFZ level-2 product, release 4) after restoring the non-tidal
149 oceanic and atmospheric background models (GAD) over ocean. The seasonal degree 1 terms
150 of the geopotential have been included (Rietbroek et al., 2009, 2011), the low degree
151 coefficients replaced with a more accurate estimate from satellite laser ranging (SLR) and the
152 high coefficients truncated to degree 100. Basin means over each ocean basin (defined as 1 on
153 sea and 0 on land) have been estimated applying a dedicated anisotropic post-processing filter
154 DDK3 (Kusche et al. 2009, Swenson and Wahr 2002). The same procedure has been applied
155 to observed and model data, e.g. to GRACE and to the hydrology model. The filtered basin
156 average of the hydrological signal is then removed from the GRACE filtered basin average to
157 obtain the hydrological-corrected seawater mass change from GRACE.

158

159 Steric-corrected sea level derived from multi-satellite (Jason-1 and Envisat) altimetry data
160 have been used to obtain an independent estimate of the ocean mass signal. To correct for the
161 steric component, maps of the steric component of sea level have been derived from the
162 oceanographic models MFSTEP (Dobricic & Pinardi 2008) in the Mediterranean Sea and
163 NEMO (Madec 2008) in the Black Sea (Grayek et al. 2010). Filtered basin averages have

164 been constructed with the same method applied to GRACE and a re-scaling factor derived
165 from the filtered and unfiltered mass estimated from steric-corrected altimetry (1.4 for the
166 Mediterranean Sea and 1.7 for the Black Sea, see Fenoglio-Marc et al., this issue). Finally, the
167 re-scaling factors have been applied to the hydrology-corrected seawater mass change
168 estimated from GRACE. The difference between the steric-corrected altimetry and the
169 hydrology-corrected GRACE seawater mass estimates allows an evaluation of the steric- and
170 continental hydrology leakage corrections.

171 **3. Results**

172 **3.1 Hydrological model results and evaluation**

173 *3.1.1 Total water storage*

174 Mean TWS, as calculated with WaterGAP3 for the period 2002 to 2009, is displayed in
175 Figure 1. The black borders show the extent of the 48 largest basins draining into the
176 Mediterranean and Black Sea. All these basins feature an area greater than 1500 km², as this
177 size has been identified to be the minimum for producing reliable results with WaterGAP3.
178 The highest TWS can be found in the Alps and Balkan Mountains, as well as in the northern
179 part of the Dnieper and Don basins, and at the eastern coast of the Black Sea. Mountainous
180 regions generally provide larger TWS as higher precipitation amounts cause higher filling
181 levels of storages. In addition, lower air temperatures in high elevations entail long duration
182 snow storages. Furthermore, large rivers, such as the Nile, Danube, and Dnieper, also feature
183 high TWS in their river beds and riparian zones. Small TWS generally occur in arid to semi-
184 arid regions, such as Northern Africa, but also in areas with very small hydrological storage
185 compartments, as for example in large coastal parts of Greece. TWS can strongly be affected
186 by anthropogenic water abstraction and consumption, which can also alter the hydrological
187 runoff regimes of rivers. Exemplary, Figure 2 shows mean annual water withdrawals for
188 irrigation purposes. Hot spots with high intensity and large extents of irrigation systems can
189 be found in the Nile Delta, the Italian Po basin, and the Spanish Ebro basin. The Ebro basin
190 features a basin wide average TWS of 83.5 mm, whereas on average 54.7 mm have already
191 been withdrawn during the model application for irrigation requirements. Taking into account
192 a Spain-explicit irrigation project efficiency of 53% (aus der Beek et al. 2010), 29 mm have
193 been consumed by plants and 25.7 mm have remained as return flow in the Ebro basin. This

194 means that without considering irrigation water uses, TWS would have been calculated as
195 112.5 mm, which again points out the importance of considering water uses when modeling
196 hydrological water balances.

197 *3.1.2 Modeled river runoff to the Mediterranean and Black Sea*

198 Figure 3 shows monthly time series of cumulated modeled river runoff into the Black Sea.
199 WaterGAP3 generally produces higher peak flows as WaterGAP2, whereas the timing and
200 phase are similar. Peak flows are dominated by the pluvio-nival regime of the Danube River,
201 which features snowmelt- and intense rainfall induced high flows between March and May.
202 The Danube contributes 51% of the total inflow to the Black Sea, followed by Don (13.9%),
203 Dnieper (11.4%), Kuban (6.8%), Rioni (3.7%), Coruh (3.1%), Dniester (2.8%), Kizil Irmak
204 (2.1%), Sakarya (1.9%), Yesil Irmak (1.8%), Filyos (1.0%) and Bug (0.8%). A comparison
205 with Dai et al. (2009) and a literature review conducted by Ludwig et al. (2009) yields a range
206 of inflow into the Black Sea of 348 to 473 km³ per year. WaterGAP3 calculated an average
207 inflow for 2002 to 2009 of 406 km³ per year, which is close to the 403 km³ per year estimated
208 by Ludwig et al. (2009) for the period 1991 to 2000 (WaterGAP3: 337 km³ per year).
209 WaterGAP2 simulates an average cumulated inflow into the Black Sea of 326 km³ per year,
210 which is below the literature review based range mentioned above. This is expected to be
211 caused by the generally small base flow produced in late summer. Differences in the results of
212 the models can be explained by the differences in model structures and drivers mentioned in
213 chapter 2.1. Especially, the spatial sub-grid resolution of 400 m x 400 m of the WaterGAP3
214 snow module reacts more dynamically and sensitive to air temperature changes, compared to
215 WaterGAP2 with a spatial resolution of 50 km x 50 km (Verzano & Menzel 2009). The
216 higher spatial resolution can cause higher snowmelt induced peak flows, as the sub grid cells
217 provide individual snow storage volumes based on elevation, albedo and climatic drivers. In
218 general, WaterGAP2 produces 19% less inflow to the Black Sea than WaterGAP3. Potential
219 sources for this discrepancy might be found in the application of different precipitation inputs,
220 as well as in the station correction factor of WaterGAP2, which can lead to negative water
221 balances, as it manipulates the water balance in order to fit modeled to observed river runoff.
222 Furthermore, WaterGAP2 applies constant water withdrawals for 2002 to 2009, which can
223 lead to the overestimation of water consumption, especially in dry seasons when precipitation
224 amounts are low. The allocation of irrigated areas in WaterGAP2 relies on the concept of
225 irrigating areas which are potentially equipped for irrigation (Döll & Siebert 2002), whereas

226 in WaterGAP3 irrigated areas have been adjusted to national statistics and reported areas (Aus
227 der Beek et al. 2010). Thus, irrigation water withdrawals are likely to be overestimated by
228 WaterGAP2. This might also explain the lower base flow in late summer modeled with
229 WaterGAP2, as most water withdrawals for irrigation purposes occur in hot and dry summer
230 months.

231 Figure 4 depicts monthly time series of cumulated modeled river runoff to the Mediterranean
232 Sea. Similar to the inflow to the Black Sea (see Figure 3), peaks modeled with WaterGAP3
233 are higher than from WaterGAP2, whereas the latter generates lower base flows. The river
234 basins draining into the Mediterranean Sea are generally smaller than those of the Black Sea
235 (see Figure 1). Here, the advantages of the fine spatial resolution of WaterGAP3 take effect.
236 Most river basins are smaller than 15000 km², which is thought to be the minimum basin size
237 for WaterGAP2 to yield realistic results; as its cell areas are approximately 2500 km² per grid
238 cell. Thus, WaterGAP3, with a cell size of about 50 km², offers the ideal setting for a
239 comprehensive model study for the Mediterranean River basins. WaterGAP3 calculates a
240 mean annual cumulated inflow to the Mediterranean Sea of 518 km³ per year for the period
241 2002 to 2009, which is in the middle of the literature review based range of Ludwig et al.
242 (2009) of 305 to 737 km³ per year. WaterGAP2 simulates about 337 km³ per year, whereas
243 similar reasons as for the difference between both models in the Black Sea basins apply. The
244 hydrological and water use system of the Nile River is very difficult to represent in a large
245 scale hydrological model, as no data about river runoff, water withdrawals and dam
246 management is available for the downstream area and Delta of the Nile. In detail, the
247 reservoirs Aswan High Dam and Lake Nasser heavily influence the river runoff, and high
248 intense double to triple cropping irrigation projects in the Nile Delta cause massive water
249 withdrawals. In addition, the Egyptian part of the Nile River provides water to more than 121
250 million people, as 95% of all Egyptians live within 20 km distance of the Nile River. These
251 water withdrawals have been included in this study. However, as no reported data about
252 domestic water withdrawals in Egypt is available, it is difficult to verify these WaterGAP3
253 model results.

254 Modeled natural flows without anthropogenic interaction exceed 300 km³ per year, whereas
255 literature values for present Nile runoff into the Mediterranean Sea range between 6 (Abu El
256 Ella 1993) and 15 (Nixon 2003) km³ per year. These large discrepancies can currently not
257 realistically be modeled with WaterGAP3. However, the TWS from Figure 1 are still realistic
258 for the Nile, as a comparison of modeled with observed runoff in the Blue and White Nile

259 sub-basins feature a very high level of agreement ($R^2 = 0.89$; Model efficiency = 0.68 at
260 GRDC station “Roseires”). Therefore, in many studies as well as in Figure 2 the Nile is
261 excluded from the cumulated inflow to the Mediterranean Sea. Without the Nile, WaterGAP3
262 simulates an average cumulated inflow for 2002 to 2009 of 318 km³ per year, which is close
263 to the 312 km³ per year Ludwig et al. (2009) have reported for the period 1991 to 2000.
264 Generally, WaterGAP3 generates 35% more inflow to the Mediterranean Sea than
265 WaterGAP2. This can again be explained by similar reasons as for the Black Sea because the
266 alpine river catchments with snowmelt and rainfall induced floods dominate the total inflow
267 to the Mediterranean Sea. The Po River accounts for 24.2% of the cumulated inflow, followed
268 by the Rhone (23.6%), Ebro (6.1%), Drin-Buna (4.1%), Orontes (3.6%), Maritsa (3.6%),
269 Adige (3.5%), Moutouya (3.5%), Simav (3.2%), and other smaller rivers which individually
270 contribute less than 3%.

271 *3.1.3 Comparison of WaterGAP3 with other hydrological models and data*

272 The results of the river runoff provided by WaterGAP3 for the Black Sea have been compared
273 in terms of the total amount to those from semi-climatological estimates (Grayek et al 2010)
274 and in terms shares from individual drainage regions to values from literature (Jaoshvili
275 2002). The comparison of the contributions from surrounding countries and correspondingly
276 assigned WaterGAP3 river runoff are shown in Figure 5 and 6, respectively. As expected, the
277 annual and inter-annual variation of total river runoff derived from the semi-climatological
278 estimate (Figure 5) is much smaller than the variation simulated by WaterGAP3. Furthermore,
279 the comparison of annual mean values from both datasets reveals that the simulated data gives
280 in general higher values than the estimated data. The difference here reaches from 1500 to
281 4000 m³/s. In Figure 6, the contributions of the individual drainage regions from surrounding
282 countries are shown. With one exception, which is the runoff of Georgia's rivers, the
283 simulated percentage shares from drainage areas vary roughly around the climatological value
284 from Jaoschvili (2002). The share of Georgian rivers in WaterGAP3 is significantly lower
285 than in the climatology and, correspondingly, the temporal mean values of the other drainage
286 regions are slightly higher than the climatological one. This can be explained by
287 anthropological effects, such as reservoir management and water withdrawals, e.g. in the
288 Kuban River basin (Ludwig et al .2009).

289 Figure 7 shows a comparison of modeled river runoff from three different hydrological
290 models with observed river runoff at the GRDC Station “Ceatal Izmail” (ID 6742900) of the

291 Danube River. This station has been selected from the 63 stations of this study, as routed river
292 runoff from GLDAS was only available for this station and for a station at the Dnieper River.
293 However, river runoff at the Dnieper station is heavily regulated, which makes it difficult to
294 judge the goodness of three models in this study. The performance of the models is evaluated
295 by calculating the coefficient of determination R^2 and the Nash-Sutcliffe efficiency NSE
296 (Nash & Sutcliffe 1970). WaterGAP3 generally yields the best fit of all three models ($R^2 =$
297 0.67 , $NSE = 0.50$). Especially, the observed volumes of peak flows are very well represented
298 by WaterGAP3, whereas the timing and phase also show a good fit to observed values. The
299 second model, WaterGAP2, features a somewhat lower goodness of fit ($R^2 = 0.47$, $NSE = -$
300 1.24), which again is caused by the underestimation of base flows. In particular, during the
301 flood event of winter 1993/1994, WaterGAP2 simulates a strong decline in runoff, whereas
302 observed runoff increases to the highest flood event of the year. This may be explained by
303 rain-on-snow conditions, which can easily set free large amounts of water, due to rapid
304 melting snow packs and frozen soil inducing Hortonian overland flow. These events are very
305 difficult to be represented in a model, especially with a spatial resolution of 0.5° . The last
306 model, GLDAS, generates runoff which is within a reasonable range ($R^2 = 0.06$, $NSE = -2.49$)
307 in terms of runoff volume, whereas the inaccurate timing and phase of modeled runoff point
308 at model structure deficiencies. However, it needs to be mentioned that both WaterGAP
309 models have been calibrated with one simple parameter (Döll et al. 2003) to observed runoff,
310 whereas all four GLDAS LSMs have not been calibrated.

311 A comparison of the goodness of WaterGAP2 and WaterGAP3 with observed data from all
312 river discharge gauging stations available in the Mediterranean and Black Sea basins is shown
313 in Figure 8. For each year the correlation between modeled and observed river runoff (in m^3)
314 has been calculated separately for each station on a monthly basis. Then, an annual
315 unweighted arithmetic mean from all available stations has been calculated. The comparison
316 shows generally higher coefficients of determination for WaterGAP3 in the range of 0.50 to
317 0.54, whereas WaterGAP2 features values between 0.44 and 0.47. For the period 2004 to
318 2007 WaterGAP2 yields better results than for the period 1992 to 2003. This can be explained
319 by the small number of gauging stations during 2004 to 2007, which are dominantly allocated
320 in large river basins. Due to the coarse spatial resolution of WaterGAP2 these basins can
321 better be represented than the average Mediterranean and Black Sea basin. Once again, the
322 reasons for the discrepancy between both models can be found in the different spatial
323 resolution and model structures mentioned in chapter 2.1.

324 3.2 Sea-mass variation validation

325 For ocean mass estimates, the amount of continental hydrological leakage which is present in
326 the GRACE basin averages after application of the post-processing filter, depends on the filter
327 smoothing and increases with the radius of the filter. Of course, it also depends on the
328 hydrological model used. The annual amplitudes of the leakage computed from the three
329 global models GLDAS, LAD and WaterGAP2 using the DDK3 filter are significantly
330 different (Table 1). Depending on the model chosen, it ranges between 7 and 23 mm in the
331 Mediterranean Sea and between 24 and 63 mm in the Black Sea. The phase of the annual
332 component is between 41 and 55 degree in the Mediterranean Sea and between 50 and 60
333 degrees in the Black Sea. The semi-annual component is almost absent in the Mediterranean
334 Sea and is small in the Black Sea.

335

336 In Fenoglio-Marc et al. (this issue) we have been using a version of the global model
337 WaterGAP2 with a native resolution of 0.5° to estimate the leakage caused by hydrology of
338 the GRACE signal. We extend here the analysis including the regional model WaterGAP3. In
339 the Mediterranean Sea the annual amplitude of the continental hydrological leakage is smaller
340 when computed from WaterGAP3 (14 +/- 3 mm) than when from WaterGAP2 (19 +/- 3 mm)
341 and peaks in both cases around the 15th February (Table 2, Figure 9). Also in the Black Sea
342 the annual amplitude corresponding to WaterGAP3 is smaller (29 +/- 5 mm) compared to the
343 amplitude corresponding to WaterGAP2 (39 +/- 5 mm) and peaks one week earlier around the
344 20th of February (Table 3, Figure 9).

345

346 The seawater mass (SLV_{mass}) has been obtained by correcting the GRACE/GFZ solution for
347 the continental hydrology leakage computed from WaterGAP3 and WaterGAP2 and by re-
348 scaling as described in section 2.2. The agreement between this GRACE-derived SLV_{mass}
349 (indicated here also with “G-h”) and the SLV_{mass} derived from steric-corrected altimetry
350 (indicated here also with “a-s”) is higher in the Mediterranean Sea than in the Black Sea,
351 independently from the hydrology model used. In both basins the agreement is higher when
352 the WaterGAP2 model is used.

353

354 In the Mediterranean Sea correlation and RMS differences of the monthly time-series are 0.83
355 and 21 mm with WaterGAP3 and 0.86 and 40 mm with WaterGAP2 (Figure 10). The annual
356 signals are comparable and, using WaterGAP2, the GRACE-derived SLV_{mass} (annual

357 amplitude 27 +/- 3 mm peaking on the 18th November) is consistent within the altimetry-
358 derived SLV_{mass} , (annual amplitude 23 +/- 3 mm peaking on the 24th November) within 3 mm
359 and 23 days. With WaterGAP3, the SLV_{mass} has annual amplitude of 35 +/- 4 mm peaking on
360 the 29th December. The higher disagreement (12 mm and 35 days) is due to the smaller
361 amplitude of WaterGAP3. As shown in Fenoglio et al. (this issue) a continental hydrological
362 correction bigger than the correction provided by WaterGAP2 is required when using the
363 MFSTEP steric correction. Figure 11 (top) depicts annual amplitudes and phases for each of
364 parameters entering in the computation of SLV_{mass} and shows the amplitude and phase (h,
365 bleu) of the rescaled hydrology component (34 mm, peaking on the 16th February) that best
366 agrees with the selected altimetry, GRACE data and MFSTEP model.

367

368 In the Black Sea correlation and RMS differences of the seawater mass SLV_{mass} monthly
369 time-series are 0.74 and 90 mm with WaterGAP3 and 0.71 and 122 mm with WaterGAP2
370 (Figure 10). Differences in annual amplitude and phase are smaller (3 mm and 9 days) with
371 WaterGAP2. The altimetry-derived SLV_{mass} (annual amplitude 32 +/- 5 mm peaking on the
372 20nd April) agrees with the SLV_{mass} from WaterGAP3 and GRACE (annual amplitude 55 +/- 4
373 mm peaking on April 1st) within 23 mm and 20 days. The lower consistency is due, also in
374 this case, to the smaller amplitude of WaterGAP3, as a higher amplitude of the continental
375 hydrological correction is needed when using the NEMO steric correction (Table 3). Figure
376 11 (bottom) depicts annual amplitudes and phases for each parameters and shows amplitude
377 and phase (h, blue) of the rescaled hydrology component (74 mm peaking on the 21st
378 February) which best agrees with the given observations from altimetry and GRACE and with
379 the NEMO steric correction.

380 **4. Conclusions and discussion**

381 This interdisciplinary study shows that WaterGAP3 produces improved estimates of total
382 water storage in the Mediterranean and Black Sea watersheds. Concerning the inflow to the
383 Black Sea the Danube provides more than 50% of the total inflow, followed by Don, Dnieper,
384 and Kuban. Generally, the inflow is peaking during spring due to snow melt conditions
385 followed by a smaller rainfall induced peak in late autumn. The inflow to the Mediterranean
386 Sea is dominated by the Po and Rhone rivers which each contribute about 25% of the total
387 inflow, whereas peak flow mostly occurs in winter. Hydrological inflow to the Mediterranean
388 and Black Sea as modeled with WaterGAP3 generally yields good results when compared to

389 values from literature (Ludwig et al. 2009). Calculated contributions to the total runoff into
390 the Black Sea from individual discharge regions in WaterGAP3 simulations show in general a
391 good agreement to climatological estimates from Jaoshvili (2002). But results reveal a lesser
392 importance of Georgian rivers for the basin's water budget compared to climatology.

393 The comparison of modeled river runoff of the regional hydrology and water use model
394 WaterGAP3 with its global counterpart WaterGAP2 features advantages for WaterGAP3.
395 When comparing both models to observed river runoff at the 63 stations available for the
396 study region (GRDC 2004) WaterGAP3 results features a coefficient of determination which
397 is about 0.09 higher than those of WaterGAP2 until the year 2000. Thereafter, the number of
398 available station data drops and mainly stations in large river basins remain, which reduces
399 the advantage of WaterGAP3 to 0.04. One of the main reasons for the general discrepancy of
400 both models can be found in the coarse spatial resolution of WaterGAP2. Especially, in the
401 Mediterranean region, small river basins dominate the total inflow into the ocean, which
402 cannot be well represented in the global model WaterGAP2. Also, the comparison between
403 WaterGAP3 and GLDAS shows large advantages for WaterGAP3, whereas it needs to be
404 mentioned that GLDAS data only for two gauging stations in the study region has been
405 available.

406

407 We have used WaterGAP3 to compute the continental hydrology leakage correction for
408 GRACE and to derive ocean water mass variation. The comparison of the resulting GRACE-
409 derived mass change with the ocean mass variation derived from steric-corrected altimetry
410 shows a general agreement in both the Mediterranean and Black Sea. Results are however
411 slightly worse as by using WaterGAP2, due to the smaller annual amplitude of the continental
412 leakage corresponding to WaterGAP3. Similar results have been found with GLDAS-CLM
413 (Fenoglio-Marc et al. (this issue)) confirming the similarity between WaterGAP3 and
414 GLDAS. On the other hand, the altimeter-derived estimates depend on the steric correction
415 that is of course not fully perfect. We conclude that the regional model WaterGAP3 is suitable
416 to correct ocean mass changes for hydrological leakage and that both the hydrology and ocean
417 models can benefit from use of GRACE and altimetry in constraining the difference between
418 the water mass derived from the two methods. Small amplitudes and phase differences have
419 been observed and need further investigation.

420

421 The regional WaterGAP3 hydrology and water use model needs further developments to
422 include a buffer strip around the current STREMP region to ensure correct application of the
423 GRACE filters, as currently, only the river basins draining into the Mediterranean and Black
424 Sea are being considered. Improvements are planned in modeling the Nile River basin, with
425 alteration of the reservoir algorithm to reflect the maximum annual release of 15 km³ (Nixon
426 2003) of fresh water into the Mediterranean Sea. Furthermore, it needs to be checked if the
427 water uses from all five modeled sectors represent the current conditions at the downstream
428 area of the Nile River.

429

430 We finally expect that the interaction and coupling of the regional hydrology and ocean
431 models using geodetic observations will improve the models. The assimilation of GRACE
432 data in WaterGAP3 as well as the separation of the GRACE signal into different hydrological
433 storage compartments by assimilating remote sensing data will be the next steps. Important
434 improvements to the hydrology model are expected, as GRACE will provide large scale mass
435 constraints to hydrology modeling in regions where observed data are missing.

436 **Acknowledgements**

437 The authors would like to thank Andreas Güntner from GFZ Potsdam for providing
438 WaterGAP2 results, and Ben Zaitchik from the Johns Hopkins University for providing
439 GLDAS data. Also, the gratuitous provision of observed river runoff data by the GRDC is
440 highly acknowledged. We further are thankful for the comments by Laurent Longuevergne
441 and by an anonymous reviewer, which helped to improve the manuscript. This study within
442 the STREMP project has been funded by the *Deutsche Forschungsgemeinschaft* SPP1257.

443 **References**

- 444 Abu El Ella, E.M., 1993. Preliminary studies on the geochemistry of the Nile river basin,
445 Egypt, in: Kempe, S., Eisma, D., Degens, E.T. (Eds), Transport of Carbon and Minerals in
446 Major World Rivers, part 6. Mitt. Geol.-Paläont. Inst. Univ. Hamburg, SCOPE/UNEP
447 Sonderband 74, Hamburg, pp. 115-135.
- 448
- 449 Alcamo, J.M., Döll, P., Henrichs, T., Kaspar, F., Lehner, B., Rösch, T., Siebert, S., 2003.
450 Development and testing of the WaterGAP2 global model of water use and availability; Hydr.
451 Sc. 48(3), 317-37.
- 452

453 Aus der Beek, T., Teichert, E., 2008. Global Permafrost Distribution in the Past, Present and
454 Future, in: Kane, D.L., Hinkel, K.M. (Eds), Ninth International Conference on Permafrost.
455 Institute of Northern Engineering, University of Alaska Fairbanks, 1, 71-77.
456

457 Aus der Beek, T.; Flörke, M.; Lapola, D.M.; Schaldach, R., 2010. Modelling historical and
458 current irrigation water demand on the continental scale: Europe. *Adv. in Geosci.* 27, 79-85.
459

460 Aus der Beek, T.; Voß, F.; Flörke, M. 2011. Modelling the impact of Global Change on the
461 hydrological system of the Aral Sea basin. *Physics and Chemistry of the Earth* 36(13), 684-
462 695.
463

464 Chambers, D.P., 2006. Observing seasonal steric sea level variations with GRACE and
465 satellite altimetry, *J. Geophys. Res.*, 111, C03010, 13 pp, doi:10.1029/2005JC002914.
466

467 Dai, A., Qian, T., Trenberth, K. E., Milliman, J. D., 2009. Changes in continental freshwater
468 discharge from 1948-2004. *J. Climate*, 22, 2773-2791.
469

470 Dobricic, S., Pinardi, N., 2008. An oceanographic three-dimensional variational data
471 assimilation scheme. *Ocean Modelling* 22(3-4), 89-105.
472

473 Döll, P., Kaspar, F., Lehner, B., 2003. A global hydrological model for deriving water
474 availability indicators: model tuning and validation. *J. Hydrol.*, 270, 105-134.
475

476 Döll, P., Lehner, B., 2002. Validation of a new global 30-min drainage direction map. *J.*
477 *Hydrol.*, 258, 214-231.
478

479 Döll P., Siebert S., 2002. Global Modeling of Irrigation Water Requirements. *Water*
480 *Resources Research* 38(4), 8.1-8.10.
481

482 Fenoglio-Marc L., Rietbock. R., Grayek S., Becker, M., Kusche J., Stanev E., 2011. Water
483 mass variation in the Mediterranean and Black Sea; this issue.
484

485 Flörke, M., Teichert, E., Bärlund, I., 2011. Future changes of freshwater needs in European
486 power plants. *Management of Environmental Quality* 22(1), 89-104.
487

488 Flörke, M., Alcamo, J., 2005. European Outlook on Water Use, Technical Report prepared for
489 the European Environment Agency. Kongens Nytorv. 6. DK-1050. Copenhagen, DK URL:
490 <http://scenarios.ewindows.eu.org/reports/fo1949029>, 2005.
491

492 Grayek, S., Stanev, E.V., Kandilarov, R., 2010. On the Response of Black Sea Level to
493 External Forcing: Altimeter Data and Numerical Modelling. *Ocean Dyn.*, 60, 123–140.
494

495 GRDC, 2004. Long Term Mean Monthly Discharges and Annual Characteristics of selected
496 GRDC Stations. The Global Runoff Data Centre: Koblenz, Germany.
497

498 Güntner, A., 2008. Improvement of Global Hydrological Models Using GRACE Data.
499 *Surveys in Geophysics* 29(4-5), 375-397, DOI: 10.1007/s10712-008-9038-y.
500

501 Hanasaki, N., Kanae, S., Oki, T., 2006. A reservoir operation scheme for global river routing
502 models. *J. Hydrol.* 327, 22-41.
503

504 Jaoshvili, S., 2002. The rivers of the Black Sea. European Environment Agency, Copenhagen
505 (in Russian and English).
506

507 Lehner, B., Verdin, K., Jarvis, A., 2008. New global hydrography derived from spaceborne
508 elevation data, *Eos, Transactions. AGU* 89(10), 93-94, <http://hydrosheds.cr.usgs.gov> (21-Oct-
509 2008).
510

511 Ludwig, W., Dumont, E., Meybeck, M., Heussner, S., 2009. River discharges of water and
512 nutrients to the Mediterranean and Black Sea: Major drivers for ecosystem changes during
513 past and future decades? *Progress in Oceanography* 80(3-4), 199-217, doi:
514 10.1016/j.pocean.2009.02.001.
515

516 Madec, G., 2008. NEMO ocean engine. Note du Pole de modelisation. Institut Pierre-Simon
517 Laplace (IPSL), France, No 27, ISSN No 1288–1619, 217 pp.
518

519 Milly P., Shmakin, A., 2002. Global modelling of land water and energy balance, Part 1: The
520 land dynamics (lad) model. *J. of Hydrometeorology* 3(3), 283-299.
521

522 Mitchell, T.D., Jones, P.D., 2005. An improved method of constructing a database of monthly
523 climate observations and associated high resolution grids. *Int. J. of Climatology*, 25(6), 693-
524 712.
525

526 Nash, J.E., Sutcliffe, J.V., 1970. River flow forecasting through conceptual models Part 1 – A
527 discussion of principles. *J. of Hydrology* 10(3), 282-290.
528

529 Nixon, S.W., 2003. Replacing the Nile: Are Anthropogenic Nutrients Providing the Fertility
530 Once Brought to the Mediterranean by a Great River? *Ambio* 32, 30-39.
531

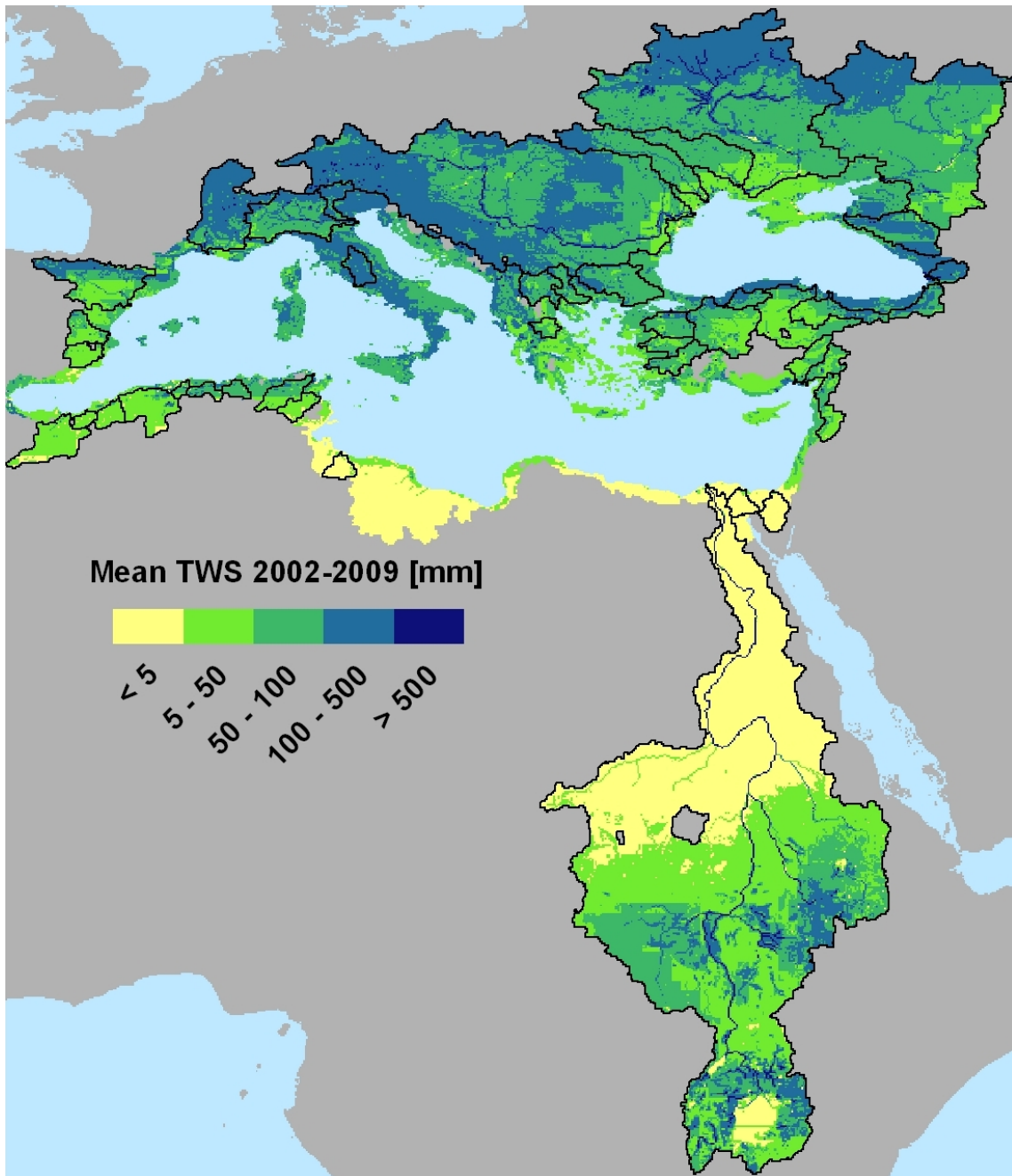
532 Rietbroek, R., Brunnabend, S.E., Dahle, C., Kusche, J., Flechtner, F., Schröter, J.,
533 Timmermann, R., 2009. Changes in total ocean mass derived from GRACE, GPS, and ocean
534 modeling with weekly resolution. *Journal Of Geophysical Research-Oceans*, 114(C11004),
535 C11004.
536

537 Rietbroek R., Fritsche, M., Brunnabend, S.-E., Daras, I., Kusche, J., Schröter, J., Flechtner, F.,
538 Dietrich, R., 2011 Global surface mass from a new combination of grace, modelled obp and
539 reprocessed gps data. *Journal of Geodynamics*, In Press, Corrected Proof, doi:
540 10.1016/j.jog.2011.02.003.
541

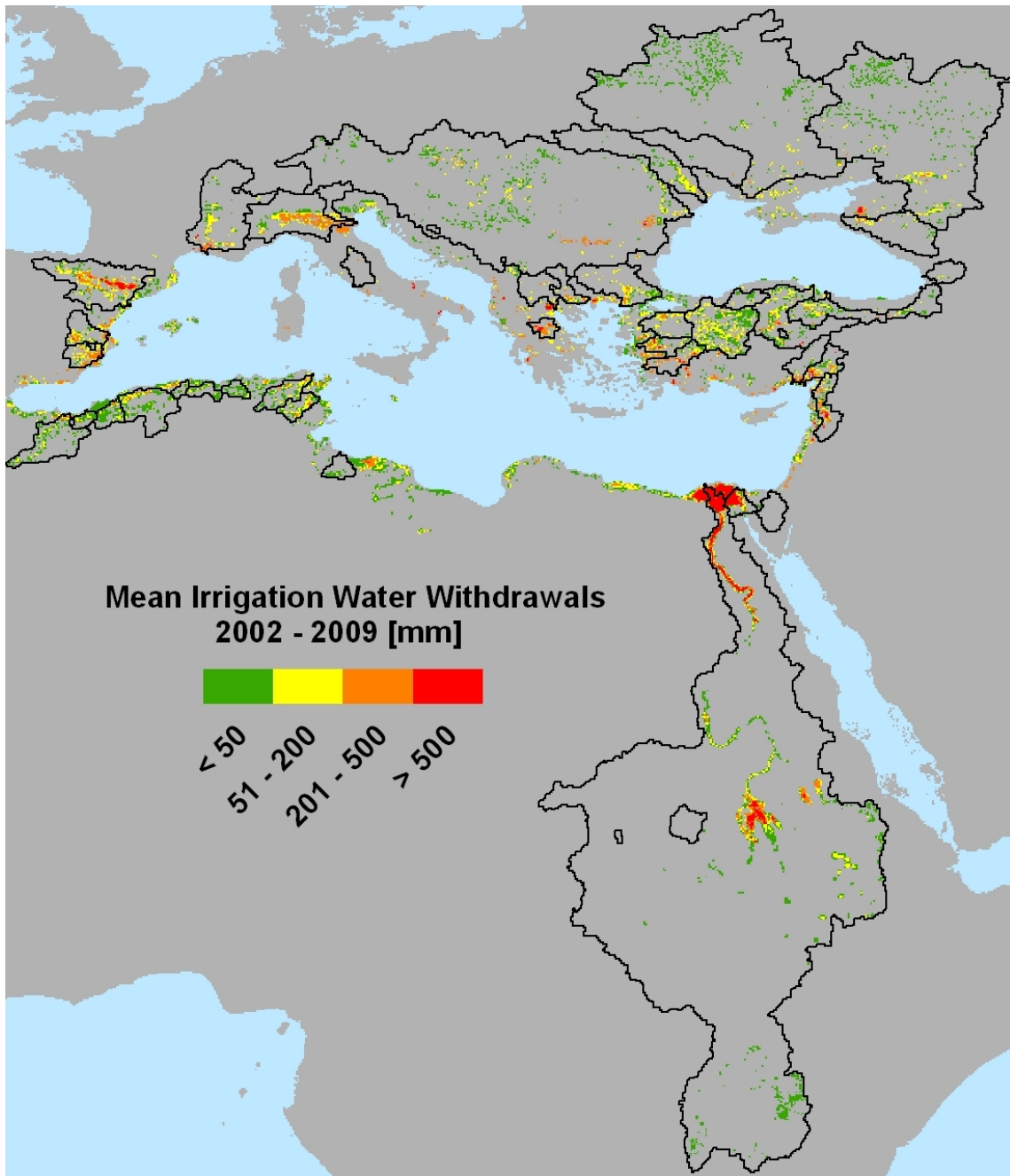
542 Rodell, M., Houser, R., Jambor, U., Gottschalck, J., Mitchell, K., Meng, C.J., Arsenault, K.,
543 Cosgrove, B., Radakovich, J., Bosilovich, M., Entin, J. K., Walker, J. P., Lohmann, D., Toll,
544 D., 2004. The global land data assimilation system. *Bull.Am. Meteorol. Soc.*, 85(3), 381–394,
545 doi:10.1175/BAMS-85-3-381.
546

547 Rudolf, B., Schneider, U., 2005. Calculation of Gridded Precipitation Data for the Global
548 Land-Surface using in-situ Gauge Observations, Proceedings of the 2nd Workshop of the

549 International Precipitation Working Group IPWG, Monterey October 2004, EUMETSAT,
550 ISBN 92-9110-070-6, ISSN 1727-432X, 231-247.
551 Schmidt, R., Schwintzer, P., Flechtner, F., Reigber, C., Güntner, A., Döll, P., Ramillien, G.,
552 Cazenave, A., Petrovic, S., Jochmann, H., Wunsch, J., 2006. GRACE observations of changes
553 in continental water storage. *Glob. Planet. Change* 50(1–2), 112–126.
554
555 Verzano, K., Hunger, M., Döll, P., 2005. Simulating river flow velocity on global scale. *Adv.*
556 *Geosci.* 5, 133-136.
557
558 Verzano, K., Menzel, L., 2009. Hydrology in Mountain Regions: Observations, Processes and
559 Dynamics. IAHS-Publication 326, Snow conditions in mountains and climate change - a
560 global view, 147–154.
561
562 Verzano, K., 2009. Climate Change Impacts on Flood Related Hydrological Processes:
563 Further Development and Application of a Global Scale Hydrological Model. Dissertation
564 University of Kassel, Germany. Available at
565 http://www.mpimet.mpg.de/fileadmin/publikationen/Reports/WEB_BzE_71_verzano.pdf
566
567 Werth, S., 2010. Calibration analysis for water storage variability of the global hydrological
568 model WGHM, *Hydrol. Earth Syst. Sci.* 14, 59-78.
569
570 Zaitchik, B. F., Rodell, M., Olivera, F., 2010. Evaluation of the Global Land Data
571 Assimilation System using global river discharge data and a source to sink routing scheme,
572 *Water Resour. Res.* 46, W06507, 17 pp, doi:10.1029/2009WR007811.

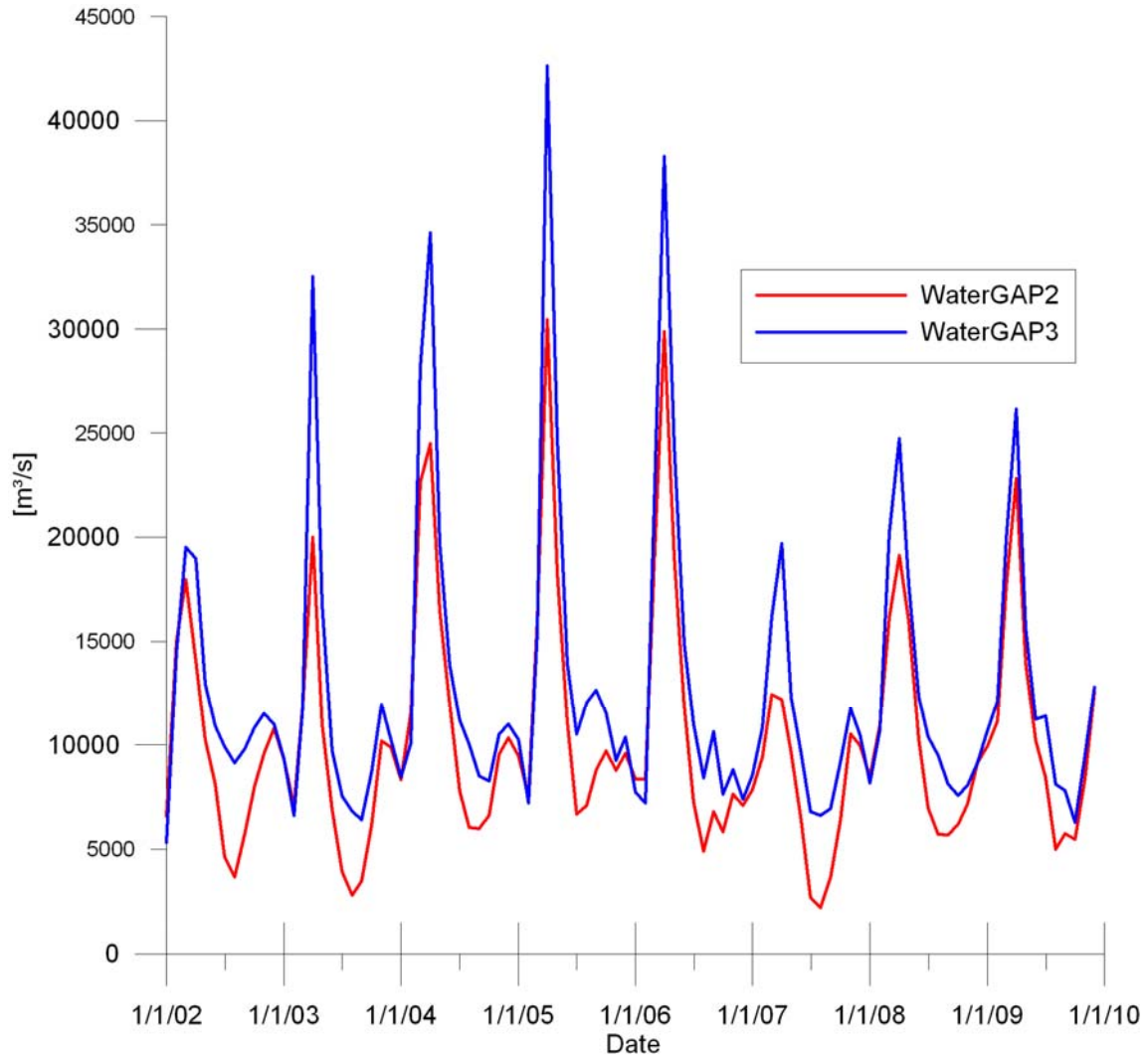


573
 574 Figure 1: Mean monthly TWS (Total Water Storage) of the Black and Mediterranean Sea
 575 river basins as simulated with WaterGAP3. Black borders show the outlines of the 40 largest
 576 rivers basins.



577

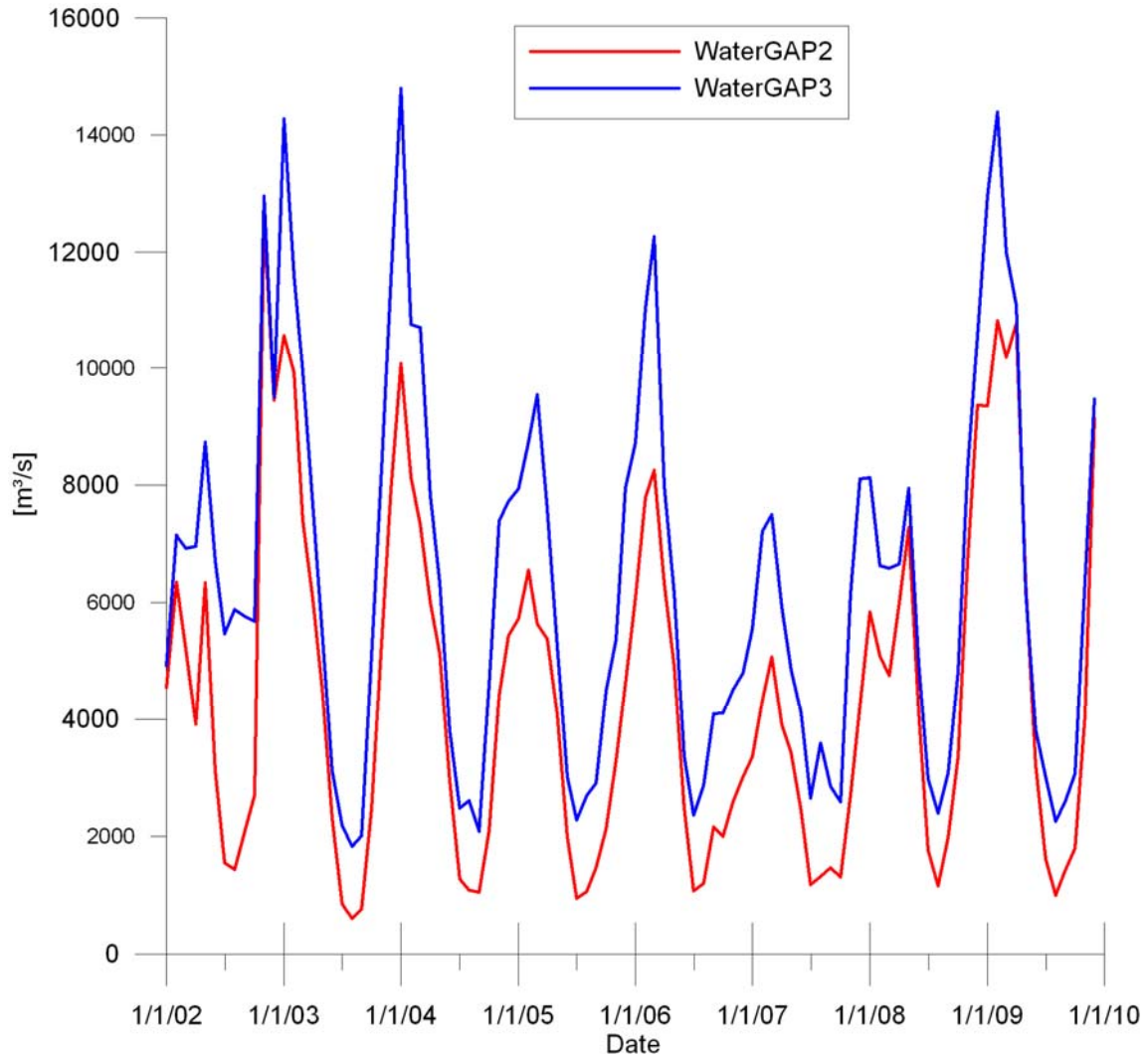
578 Figure 2: Mean annual irrigation water withdrawals as simulated with WaterGAP3.



580

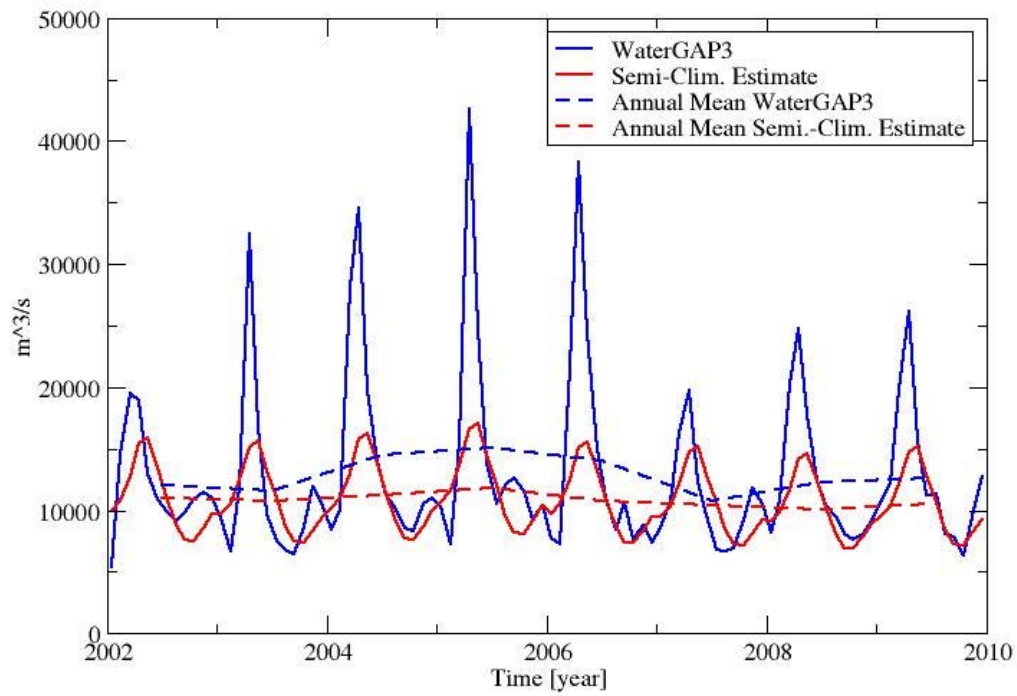
581 Figure 3: Modeled cumulated monthly inflow into the Black Sea.

582

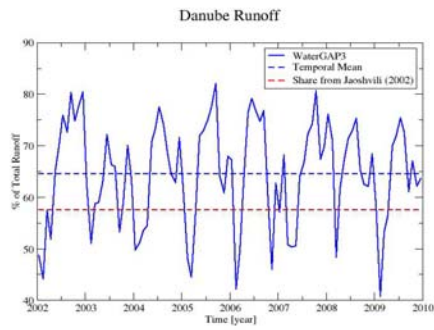


583

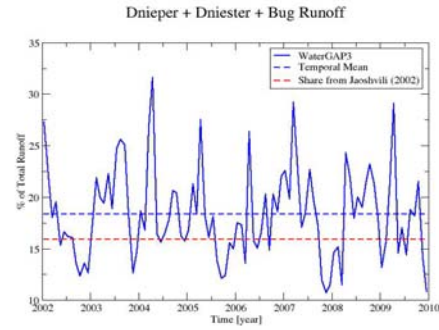
584 Figure 4: Modeled cumulated monthly inflow into the Mediterranean Sea. Nile runoff data is
585 not included due to its heavy regulation.



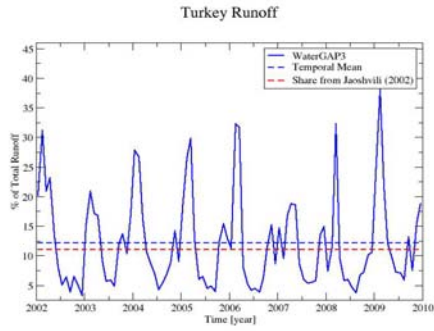
586
 587 Figure 5: Comparison of total runoff into the Black Sea from semi-climatological estimation
 588 from Grayek et al (2010) (red solid line) and from WaterGAP3 (blue solid line). The dashed
 589 lines show the corresponding annual mean of the data.
 590
 591
 592



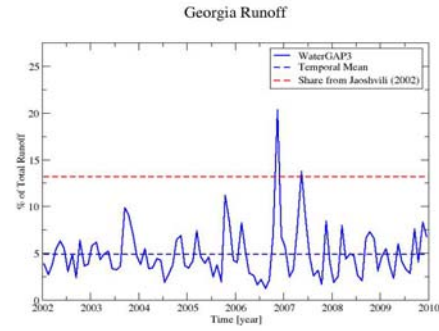
593 a)



b)



594 c)

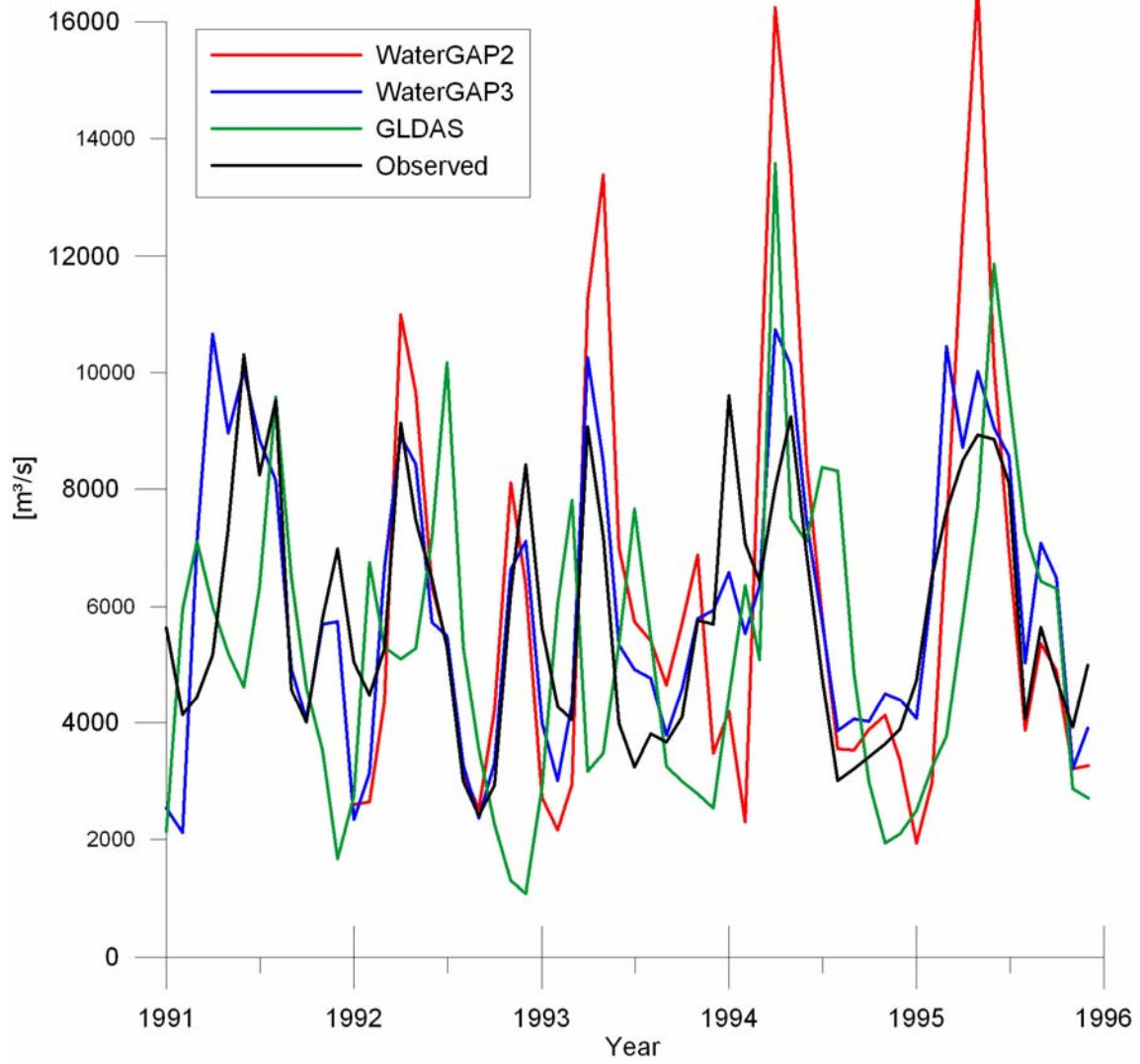


d)

595 Figure 6: Discharge shares of drainage regions from Jaoshvili (2002) calculated from
 596 WaterGAP3 output for the Black Sea (blue line) and the climatological values taken from
 597 Jaoshvili (2002) (red line). Russian rivers (1.9% of total runoff in Jaoshvili (2002)) and
 598 Bulgarian rivers (0.6% of total runoff in Jaoshvili(2002)) are not illustrated because they are
 599 not included in the present WaterGAP3 data.

600

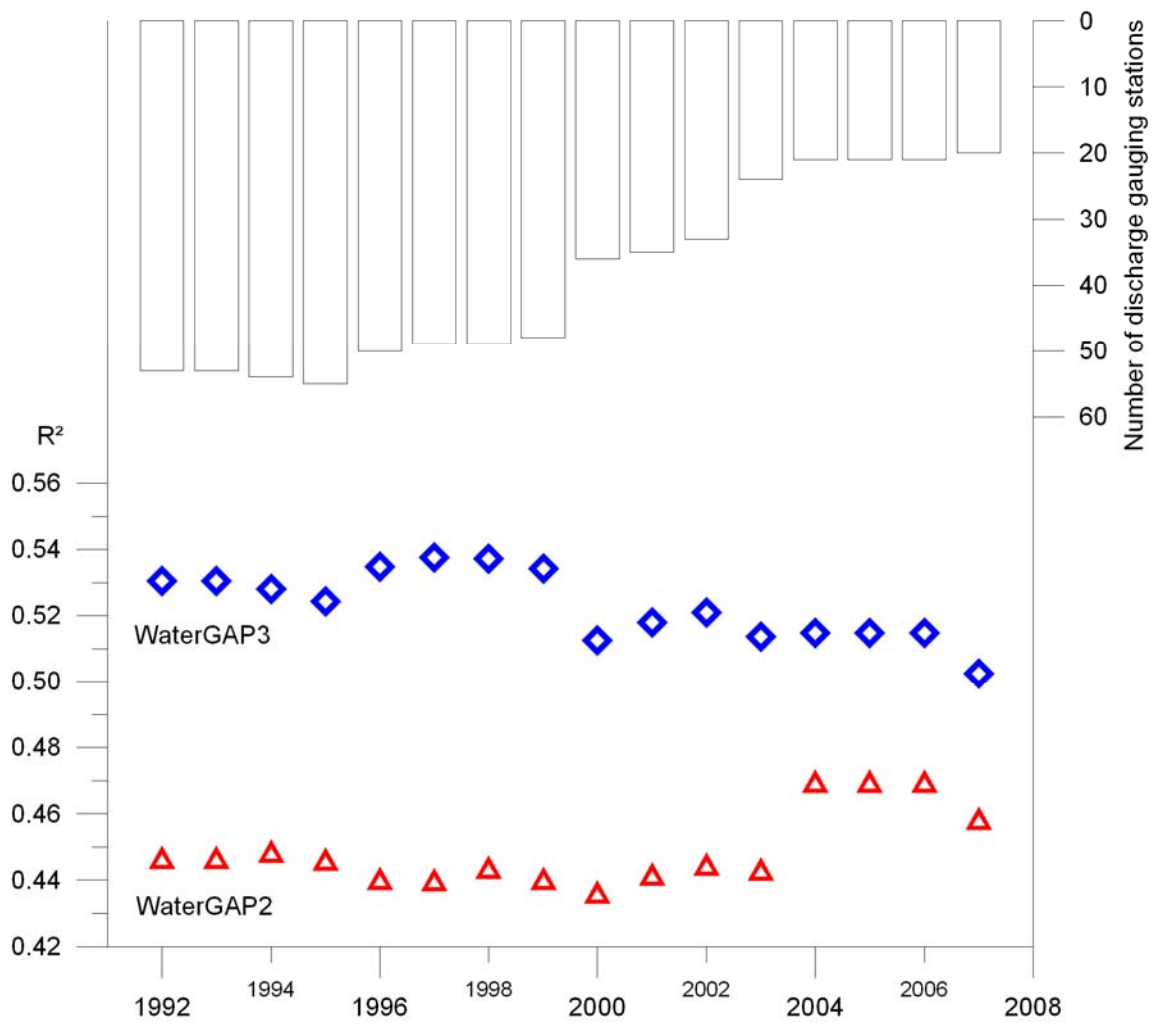
601



602

603

604 Figure 7: Comparison of modeled river runoff from two different hydrological models and a
 605 land surface model (GLDAS) with observed river runoff at the GRDC Station “Ceatal Izmail”
 606 (ID 6742900) of the Danube River.

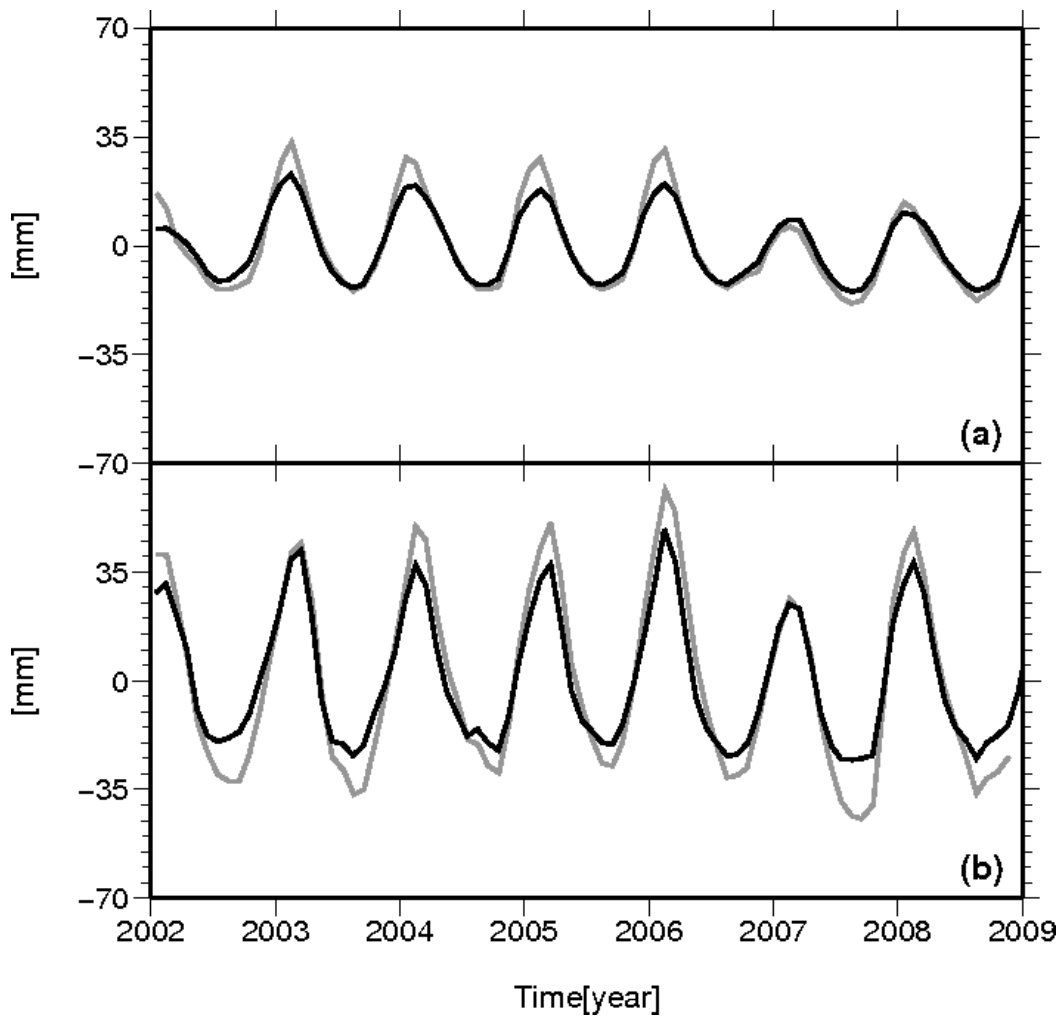


607

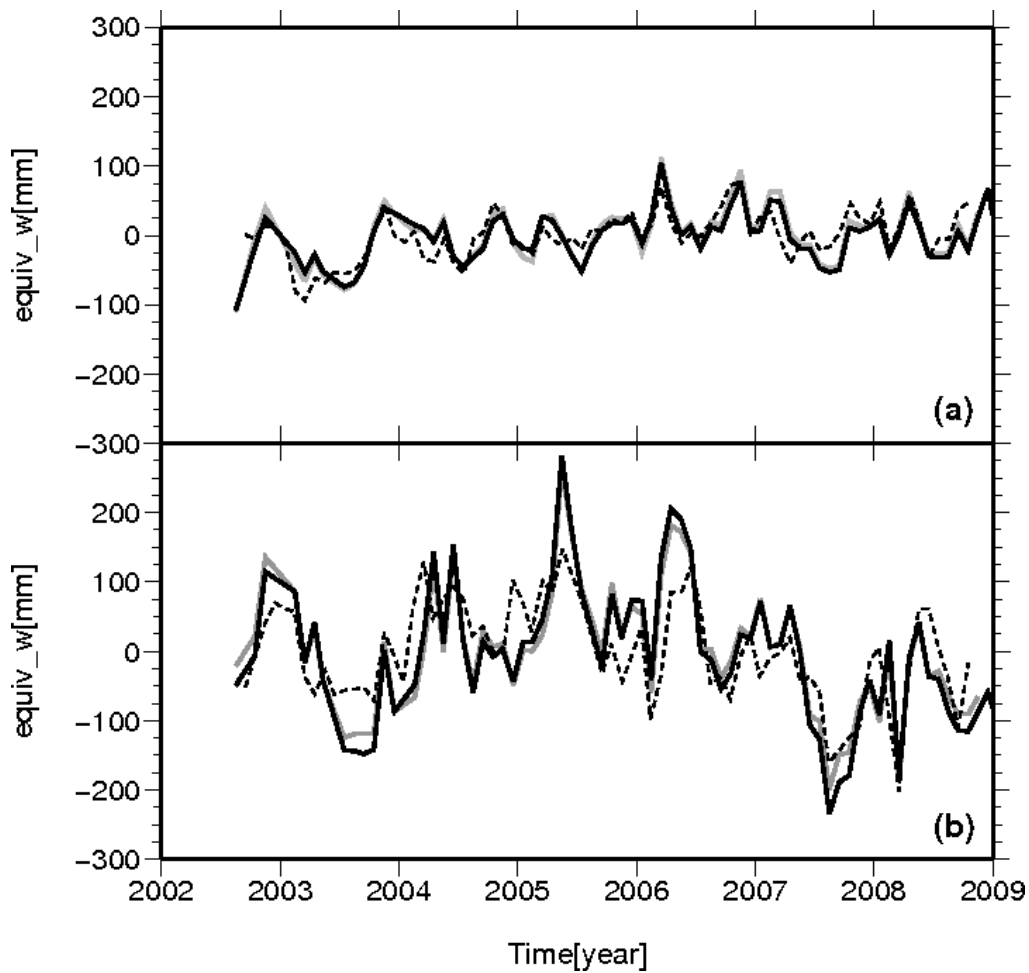
608

609

Figure 8: Evaluation of the goodness of modeled river runoff (compared to observed data) with regard to number of discharge gauging stations available.



610
 611 Figure 9: Hydrological leakage included in the seawater change estimated from GRACE in
 612 Mediterranean Sea (a) and in Black Sea (b) derived using WaterGAP2 (grey) and WaterGAP3
 613 (black). Re-scaling is not applied.
 614
 615
 616

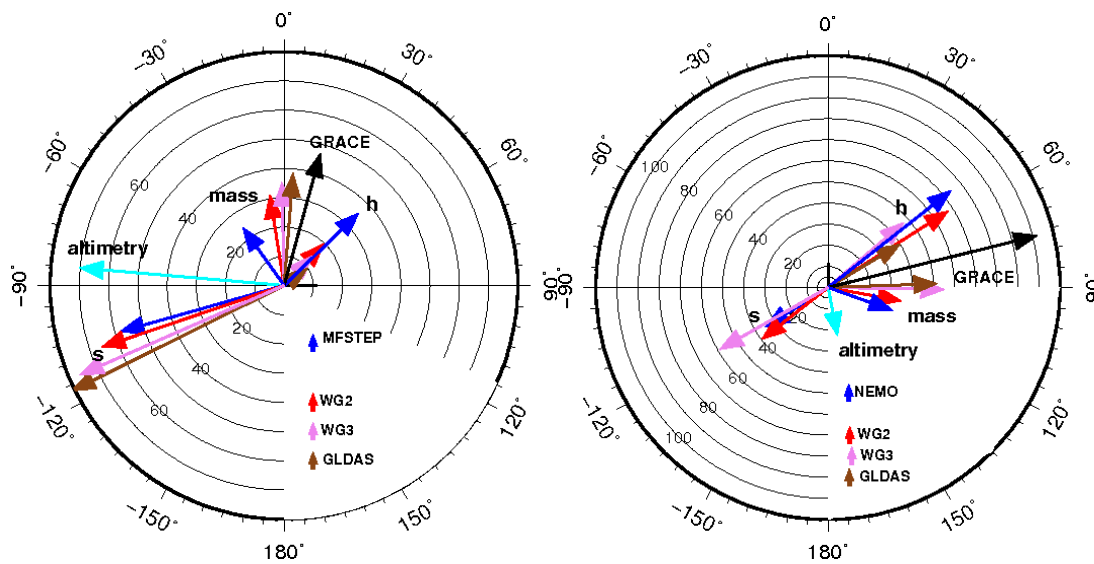


617

618 Figure 10: Basin average in Mediterranean Sea (a) and in Black Sea (b) of mass-induced sea
 619 level derived from GRACE/GFZ solutions corrected for the hydrology leakage using
 620 WaterGAP3 (black) and WaterGAP2 (grey). Mass-induced sea level derived from steric-
 621 corrected altimetry (dashed line) is also shown.

622

623



624

625 Figure 11: Annual amplitudes and phases in Mediterranean Sea (left) and Black Sea (right) of
 626 observed and derived parameters (water mass, steric correction (s) and continental hydrology
 627 correction (h)), for selected hydrology and ocean models. GRACE and altimetry basin
 628 averages are kept fixed. In each basin a regional ocean model and three hydrology models are
 629 used. Re-scaling has been applied.

630 Table 1: Annual (*A*) and semi-annual (*SA*) amplitude (*Amp*, mm) and phase (*Ph*, days) of
 631 monthly averages of hydrology leakage from different hydrology models due to filtering
 632 (DDK3) and to truncation (degree 100) in the Mediterranean (*MED*) and Black Sea (*BS*).
 633

Model	MED	MED	MED	MED	BS	BS	BS	BS
	A	A	SA	SA	A	A	SA	SA
	Amp	Ph	Amp	Ph	Amp	Ph	Amp	Ph
GLDAS-CLM01	7 +/- 3	55 +/- 22	1 +/- 3	171 +/- 4	24 +/- 3	60 +/- 7	1 +/- 3	71 +/- 58
LAD	23 +/- 3	41 +/- 8	2 +/- 3	34 +/- 2	63 +/- 3	58 +/- 3	4 +/- 3	74 +/- 24
WaterGAP2	19 +/- 3	45 +/- 8	4 +/- 3	26 +/- 2	39 +/- 3	57 +/- 4	5 +/- 4	47 +/- 12
WaterGAP3	14 +/- 3	44 +/- 11	2 +/- 3	34 +/- 20	29 +/- 5	50 +/- 6	6 +/- 3	53 +/- 13

634

635 Table 2: Annual (A) and semi-annual (SA) amplitudes (*Amp*, mm), phases (*Ph*, days) and
636 trends of monthly basin averages of water mass variation SLV_{mass} from steric-corrected
637 altimetry (*a-s*) and hydrology-corrected GRACE (*G-h*) in the Mediterranean Sea from
638 WaterGAP2 (*WG2*) and WaterGAP3 (*WG3*), continental hydrology leakage correction
639 simulated by the two models (h_{WG2} , h_{WG3}) and derived from comparison of GRACE with steric-
640 corrected altimetry, steric correction simulated by an ocean model and derived from
641 comparison of altimetry with hydrology-corrected GRACE. The re-scaling factor 1.4 has been
642 applied.
643

	A Amp (mm)	A Ph (days)	SA Amp (mm)	SA Ph (days)	Trend (mm/yr)
$SLV_{mass} = a - s_{MFS}$	24 +/- 3	329 +/- 6	13 +/- 3	119 +/- 3	8.3 +/- 3
$SLV_{mass} = \text{Scaled } (G - h_{WG2})$	27 +/- 4	352 +/- 3	19 +/- 5	123 +/- 5	5.3 +/- 2
$SLV_{mass} = \text{Scaled } (G - h_{WG3})$	35 +/- 4	364 +/- 3	17 +/- 4	125 +/- 3	5.5 +/- 2
h_{WG2}	20 +/- 3	44 +/- 6	2 +/- 3	34 +/- 3	-1.0 +/- 0.6
h_{WG3}	14 +/- 3	44 +/- 6	2 +/- 3	34 +/- 6	-1.2 +/- 6
$h = \text{Scaled } (G - a + s_{MFS})$	34 +/- 3	47 +/- 7	2 +/- 5	160 +/- 3	-8.7 +/- 2.1
s_{MFS}	58 +/- 4	258 +/- 4	1 +/- 4	86 +/- 4	-10.1 +/- 0.6
$s_{wg2} = \text{Scaled } (a - G + h_{WG2})$	66 +/- 4	255 +/- 4	6 +/- 3	31 +/- 3	-5.3 +/- 1.1
$s_{wg3} = \text{Scaled } (a - G + h_{WG3})$	76 +/- 4	250 +/- 4	5 +/- 4	50 +/- 4	-5.8 +/- 1.3

644

645

646 Table 3: as Table 2 for the Black Sea. The re-scaling factor 1.7 has been applied.
 647

	A Amp (mm)	A Ph (day)	SA Amp (mm)	SA Ph (day)	Trend (mm/yr)
$SLV_{mass} = a - s_{NEMO}$	32 +/- 5	111 +/- 10	33 +/- 3	163 +/- 10	-12.2 +/- 2
$SLV_{mass} = \text{Scaled } (G - h_{WG2})$	35 +/- 4	102 +/- 3	45 +/- 8	147 +/- 10	-12.2 +/- 2
$SLV_{mass} = \text{Scaled } (G - h_{WG3})$	55 +/- 4	92 +/- 3	49 +/- 4	148 +/- 3	-13.2 +/- 2
h_{WG2}	68 +/- 7	58 +/- 6	10 +/- 5	50 +/- 5	-0.3 +/- 2
h_{WG3}	47 +/- 3	50 +/- 6	11 +/- 3	53 +/- 6	-1.2 +/- 2
$h = \text{Scaled } (G - a + s_{NEMO})$	74 +/- 3	52 +/- 7	22 +/- 5	111 +/- 3	-2.5 +/- 2.1
s_{NEMO}	35 +/- 4	241 +/- 4	3.5 +/- 4	38 +/- 4	-0.3 +/- 0.6
$s_{wg2} = \text{Scaled } (a - G + h_{WG2})$	40 +/- 4	235 +/- 4	19 +/- 3	32 +/- 3	0.1 +/- 1.1
$s_{wg3} = \text{Scaled } (a - G + h_{WG3})$	59 +/- 4	243 +/- 4	20 +/- 4	35 +/- 4	0.5 +/- 1.3

648
 649
 650
 651